Variational calculations for anisotropic solitons in dipolar Bose-Einstein condensates

Rüdiger Eichler, Jörg Main, and Günter Wunner
Institut für Theoretische Physik 1, Universität Stuttgart, D-70550 Stuttgart, Germany
(Received 26 October 2010; published 3 May 2011)

We present variational calculations using a Gaussian trial function to calculate the ground state of the Gross-Pitaevskii equation (GPE) and to describe the dynamics of the quasi-two-dimensional solitons in dipolar Bose-Einstein condensates (BECs). Furthermore, we extend the ansatz to a linear superposition of Gaussians, improving the results for the ground state to exact agreement with numerical grid calculations using imaginary time and the split-operator method. We are able to give boundaries for the scattering length at which stable solitons may be observed in an experiment. By dynamic calculations with coupled Gaussians, we are able to describe the rather complex behavior of the thermally excited solitons. The discovery of dynamically stabilized solitons indicates the existence of such BECs at experimentally accessible temperatures.

DOI: 10.1103/PhysRevA.83.053604 PACS number(s): 03.75.Lm, 05.30.Jp, 05.45.−a

I. INTRODUCTION

Since the prediction and experimental realization of Bose-Einstein condensates (BECs), the field of cold atomic gases has been the subject of multiple theoretical and experimental investigations. BECs with long-range interaction that can be experimentally realized by the condensation of atoms with a magnetic dipole moment such as ^{52}Cr are of special interest [1–3]. To stabilize such condensates, optical traps are generally applied in all three spatial directions. However, it has been shown by Tikhonenkov *et al.* [4] that stable quasi-two-dimensional solitons are possible where a trap is applied in only one direction perpendicular to the axis of the aligned atomic dipoles.

Solitons are a nonlinear effect that arises when the dispersion and the nonlinearity cancel each other out. BEC solitons suffer from two kinds of instabilities: First, strong attractive particle interactions can cause the collapse of the condensate. Second, when the interactions are only weakly attractive or even repulsive, the BEC can dissolve in the directions where the external trap is open.

A prerequisite for the experimental realization of solitons is a detailed theoretical investigation of the range of parameters where the condensate is stable. The relevant parameters are the trap frequency, the scattering length of the contact interaction, and the excitation energy that allows for an estimation of the temperature range where the solitons can exist. Detailed analysis of the stationary states and the dynamics of solitons based on extended variational calculations is the objective of this paper.

In the mean-field approximation, the BEC with number of particles N is described by the extended Gross-Pitaevskii equation (GPE). Introducing "natural" units for mass $m_d = 2m$, action $\hbar$, length $a_d = (m\mu_0\mu^2)/(2\pi\hbar^2)$, energy $E_d = \hbar^2/(2ma_d^2)$, and frequency $\gamma_d = \hbar/(ma_d^2)$; abbreviating a_{sc}/a_d as a; and making use of the scaling properties of the GPE $(\tilde{\boldsymbol{r}},\tilde{\gamma},\tilde{t},\tilde{\psi},\tilde{E}) = (N^{-1}\boldsymbol{r},N^2\gamma,N^{-2}t,N^{3/2}\psi,NE)$ leads to the scaled, extended time-dependent GPE in "natural" units:

$$i\frac{d}{dt}\psi(\boldsymbol{r}) = \Bigg[-\Delta+\gamma_y^2y^2+8\pi a\,|\psi(\boldsymbol{r})|^2 + \int d^3r'\frac{1-3\cos^2\theta}{|\boldsymbol{r}-\boldsymbol{r}'|^3}\left|\psi(\boldsymbol{r}')\right|^2\Bigg]\psi(\boldsymbol{r}), \quad (1)$$

where the tilde is omitted. All results in this work are given in these dimensionless units. The dipole moments of the atoms are aligned in the z direction by an external magnetic field, and θ is the angle between $\boldsymbol{r}-\boldsymbol{r}'$ and the magnetic-field axis. In the trap geometry assumed here, only a trap in the y direction perpendicular to the magnetic field is present; i.e., $\gamma_x = \gamma_z = 0$.

In Ref. [4] the GPE [Eq. (1)] was solved approximately by use of a variational approach with a Gaussian-type orbital and numerically exactly by simulations on a grid. The grid calculations are numerically quite expensive. For a detailed analysis of the parameter space of quasi-two-dimensional solitons, we therefore introduce and employ an extended variational method based on coupled Gaussian functions, which has already turned out, for dipolar BECs with an axisymmetric three-dimensional trap, to be a full-fledged alternative to grid simulations [5–7]. In this paper the stable ground state of the condensate is computed by imaginary-time evolution (ITE) of an initial wave function, and it is shown that typically, three to six coupled Gaussians are sufficient to obtain fully converged results. For a given trap frequency γ_y, stable solitons exist in a finite range of the scattering length a; outside that range the condensate collapses or dissolves.

The dynamics of energetically excited solitons is studied by solving the equations of motion for the variational parameters in real time. The mean-field energy of the ground state is typically only slightly below the energy threshold where the soliton can dissolve. However, investigation of the dynamics reveals the existence of dynamically stabilized solitons at energies far above that threshold, indicating the possible experimental realization of solitons at temperature $T \approx 5\mu$K or even higher in the limit of the GPE. The transition temperature of a chromium BEC is experimentally given by $T_c \approx 700$ nK [1]. Therefore the soliton can be dynamically stabilized in all such BECs.

The paper is organized as follows. In Sec. II we will investigate the solitons with the ansatz of a single Gaussian wave packet. The appealing simplicity of this model is that both the stationary states and the dynamics of the solitons can be obtained from the Hamiltonian of a pseudoparticle moving in a three-dimensional potential. In Sec. III the variational ansatz will be extended to a linear superposition

of Gaussian wave packets (GWPs), and the time-dependent variation principle (TDVP) will be applied to GWPs. The imaginary time evolution method will be used in Sec. IV to evaluate the ground state, and the results will be compared to calculations with one Gaussian, as well as to numerical grid calculations with the split-operator method. The analysis of real-time dynamics allows us to estimate the stability of excited solitons at finite temperatures. Concluding remarks are given in Sec. V.

II. VARIATIONAL APPROACH WITH A SINGLE GAUSSIAN

Although the variational ansatz with a single Gaussian function cannot provide quantitatively correct results, the simple model already allows us to gain deep insight into the physics of the quasi-two-dimensional solitons.

The ansatz with a single Gaussian as a trial function in the TDVP reads

$$\psi(\boldsymbol{r}) = e^{i\left(A_x x^2 + A_y y^2 + A_z z^2 + \gamma\right)}, \tag{2}$$

with the complex variational parameters

$$A_\sigma = A_\sigma^r + i A_\sigma^i, \quad \sigma = x,y,z \tag{3a}$$
$$\gamma = \gamma^r + i\gamma^i. \tag{3b}$$

The parameters A_σ^i determine the real half-widths $L_\sigma = 1/\sqrt{2A_\sigma^i}$ of the Gaussian function, γ^i describes the amplitude $\hat{\mathcal{A}} = \exp(-\gamma^i)$ used for normalization of the wave function, and γ^r is a global phase. The variational ansatz [Eq. (2)], of course, strongly simplifies the problem. Nevertheless, the investigation of this model yields physical insight, and the results for the ground state are, as will be shown, qualitatively correct.

The mean-field energy and the chemical potential are

$$E_{\mathrm{mf}} = \langle -\Delta \rangle + \langle V_t \rangle + \frac{1}{2}\left(\langle V_c \rangle + \langle V_d \rangle\right) \tag{4}$$

$$\text{and} \quad \varepsilon = \langle -\Delta \rangle + \langle V_t \rangle + \langle V_c \rangle + \langle V_d \rangle, \tag{5}$$

respectively. The expectation values with the wave function ψ given in Eq. (2) are

$$\langle -\Delta \rangle = A_x^i + A_y^i + A_z^i + \frac{\left(A_x^r\right)^2}{A_x^i} + \frac{\left(A_y^r\right)^2}{A_y^i} + \frac{\left(A_z^r\right)^2}{A_z^i} \tag{6}$$

for the kinetic term,

$$\langle V_t \rangle = \frac{1}{4}\left(\frac{\gamma_x^2}{A_x^i} + \frac{\gamma_y^2}{A_y^i} + \frac{\gamma_z^2}{A_z^i}\right) \tag{7}$$

for the trapping potential,

$$\langle V_c \rangle = 8a\sqrt{\frac{A_x^i A_y^i A_z^i}{\pi}} \tag{8}$$

for the scattering potential, and

$$\langle V_d \rangle = \sqrt{\frac{A_x^i A_y^i A_z^i}{\pi^3}}\left(\frac{4\pi}{3}\left[\kappa_x\kappa_y R_D\left(\kappa_x^2,\kappa_y^2,1\right) - 1\right]\right) \tag{9}$$

for the dipolar potential, with $\kappa_x = \sqrt{A_z^i/A_x^i}$ and $\kappa_y = \sqrt{A_z^i/A_y^i}$. The term

$$R_D(x,y,z) = \frac{3}{2}\int_0^\infty \frac{dt}{\sqrt{(x+t)(y+t)(z+t)^3}} \tag{10}$$

denotes an elliptic integral of the second kind in "Carlson's form," which can be evaluated with a fast and stable approximation algorithm [8,9] more efficiently than with the integral representation given in Ref. [4].

A. Hamiltonian form of the equations of motion

The ground state of the GPE can, in principle, be obtained by minimizing the mean-field energy in Eq. (4). Alternatively, the TDVP can be applied to derive equations of motion for the variational parameters in Eq. (3). The equations of motion can be used to investigate the dynamics of the soliton, and we can find the stationary states of the system by searching for the fixed points of these equations. The stable fixed point with the lowest mean-field energy denotes the ground state.

For the ansatz of a single Gaussian the system can be transformed to the descriptive form of a Hamiltonian system by the coordinate transformation

$$A_\sigma^r = \frac{p_\sigma}{4q_\sigma}, \quad A_\sigma^i = \frac{1}{8q_\sigma^2}, \quad \sigma = x,y,z. \tag{11}$$

The Hamiltonian in the $(\boldsymbol{q},\boldsymbol{p})$ coordinates

$$H = \frac{p_x^2 + p_y^2 + p_z^2}{2} + \frac{1}{8q_x^2} + \frac{1}{8q_y^2} + \frac{1}{8q_z^2} + 2\gamma_y^2 q_y^2 + \frac{\sqrt{\frac{2}{\pi}}a}{8q_x q_y q_z} + \frac{1}{24\sqrt{2\pi}q_z}\left[\frac{1}{q_z^2}R_D\left(\frac{q_x^2}{q_z^2},\frac{q_y^2}{q_z^2},1\right) - \frac{1}{q_x q_y}\right] \tag{12}$$

has the conventional form $H = T + V_h$. It can be shown that Hamilton's equations

$$\dot{\boldsymbol{q}} = \frac{\partial H}{\partial \boldsymbol{p}} = \boldsymbol{p}, \quad \dot{\boldsymbol{p}} = -\frac{\partial H}{\partial \boldsymbol{q}} = -\frac{\partial V_{\mathrm{h}}}{\partial \boldsymbol{q}} \tag{13}$$

lead to the same equations of motion as the TDVP applied to the variational parameters in Eq. (3).

The potential V_h is visualized in Fig. 1. The isopotential surfaces close to the stable fixed point have an ellipsoidal form. At the trap energy $E_{\mathrm{mf}} = \gamma_y$, the potential becomes open. The unstable fixed point at values of q_y smaller than the local minimum is given by the saddle point where the surrounding isosurfaces have hyperbolic form. In Fig. 1(c) the potential at a smaller scattering length close to the bifurcation point is shown. The local minimum and the saddle point approach one another and coincide at the critical scattering length a_{crit}.

B. Stationary states and linear stability

The fixed points of the system can now be easily calculated by a nonlinear root search for $\dot{\boldsymbol{q}} = 0$ and $\dot{\boldsymbol{p}} = 0$ in Hamilton's equations [Eq. (13)]. In Fig. 2, the mean-field energy and the chemical potential of the stable ground state and of an excited unstable state are shown as functions of the scattering

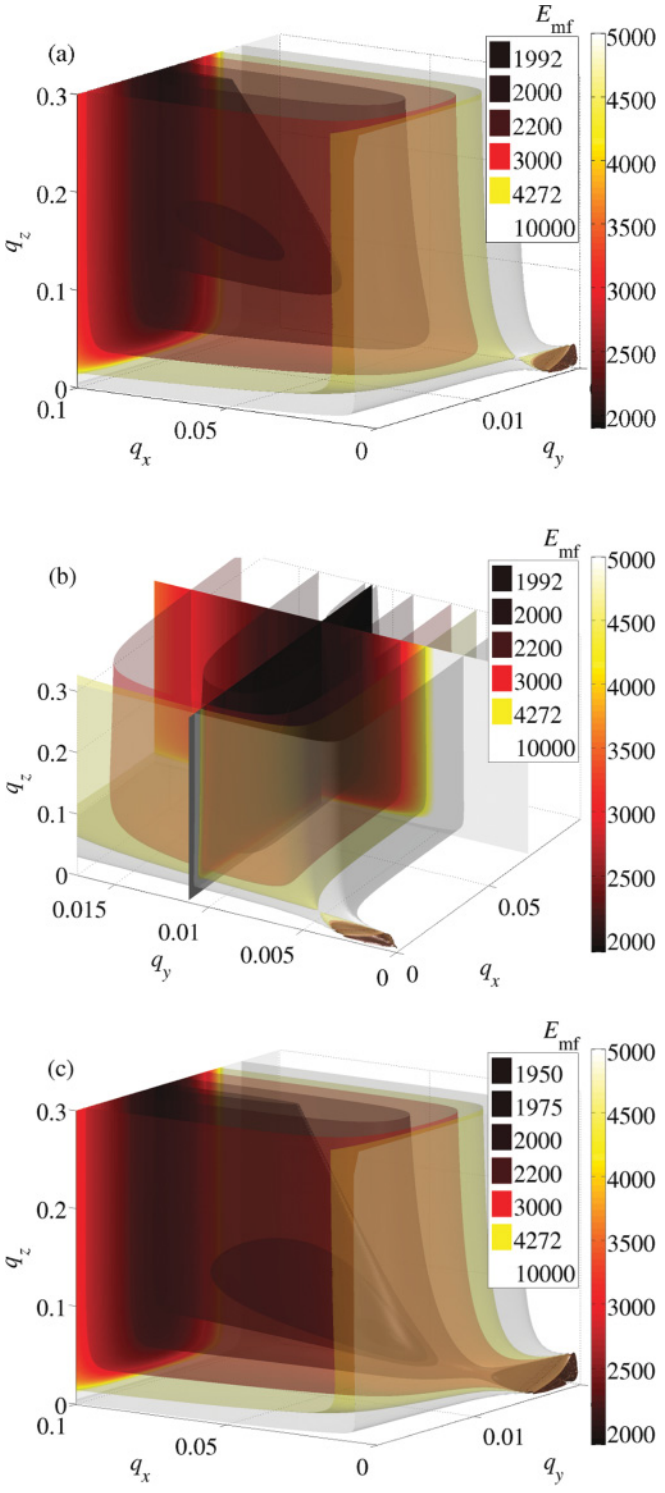

FIG. 1. (Color online) Three-dimensional potential $V_h(\boldsymbol{q})$ for $\gamma_y = 2000$ visualized by isosurfaces. (a) Scattering length $a = 0.1$. The ellipsoidal form of the isosurfaces marks the stable minimum, and the hyperbolic form of the isosurfaces close to zero marks the saddle point. In (b) the potential is rotated to show that the saddle point lies at smaller q_y values than the minimum. (c) Same as (a) but at scattering length $a = 0.08$, lowered toward the bifurcation point. The minimum and the saddle point approach each other.

length. The two branches emerge in a tangent bifurcation at the critical scattering length a_{crit}. In Fig. 2(c) the width

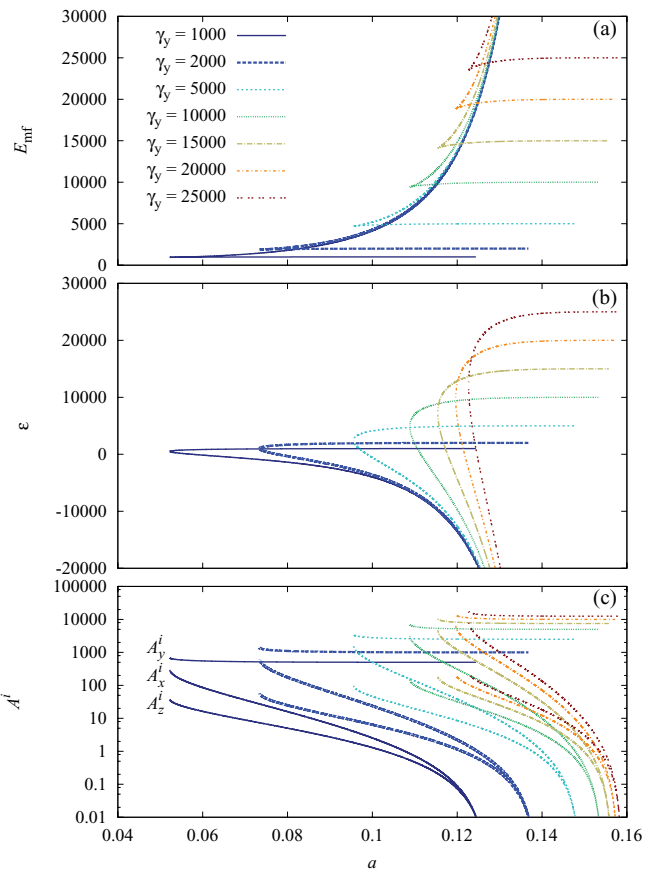

FIG. 2. (Color online) Mean-field energy (a), chemical potential (b), and width parameters of the trial function for the stable ground state on a logarithmic scale (c) as functions of the scattering length for different values of trap frequencies.

parameters corresponding to the ground state show that, with increasing scattering length, the soliton gets very broad and finally dissolves.

To analyze the stability of the solution of the GPE, the eigenvalues Λ of the six-dimensional Jacobi matrix

$$J = \left.\frac{\partial\left(\dot{A}^r_\sigma, \dot{A}^i_\sigma\right)}{\partial\left(A^r_\sigma, A^i_\sigma\right)}\right|_{\dot{A}_\sigma = 0}, \quad \sigma = x, y, z, \tag{14}$$

or equivalently in the canonical coordinates, the eigenvalues $-\Lambda^2$ of the three-dimensional real symmetric Hesse matrix $\partial^2 V_h / \partial \boldsymbol{q}^2|_{\nabla V_h = 0}$ of the potential $V_h(\boldsymbol{q})$ are calculated. The results are shown in Fig. 3. The eigenvalues appear in pairs of different sign and are all purely imaginary for the stable state. The linear stability for different trap frequencies shows qualitatively similar behavior.

C. Dynamics with a frozen Gaussian

Hamilton's equations [Eq. (13)] describe the dynamics of the soliton with the potential $V_h(\boldsymbol{q})$. The systematic investigation and visualization of the dynamics of a Hamiltonian system with three degrees of freedom is a nontrivial task. However, the force in the y direction is dominated by the strong harmonic-trap potential. If, therefore, γ_y is sufficiently large, at least for the ground state of the condensate,

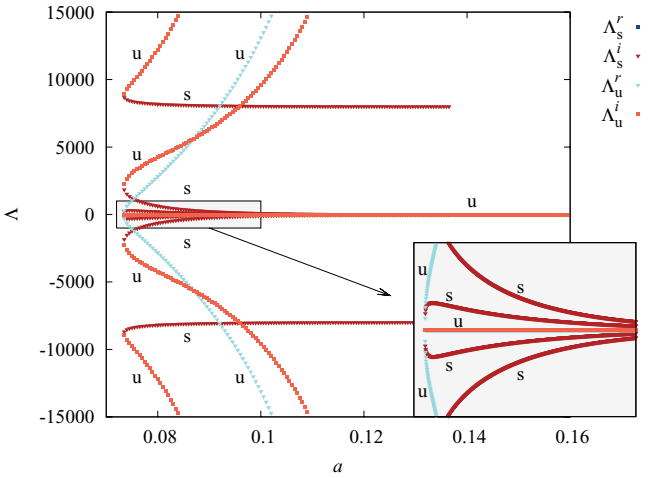

FIG. 3. (Color online) Real and imaginary parts of the eigenvalues of the Jacobi matrix J as a function of the scattering length for the trap frequency $\gamma_y = 2000$. The stable branch shows purely imaginary eigenvalues; the unstable one has nonvanishing real parts. The eigenvalues of the stable Λ_s and unstable branch Λ_u coincide at the bifurcation point. The inset shows a magnification of the rectangle.

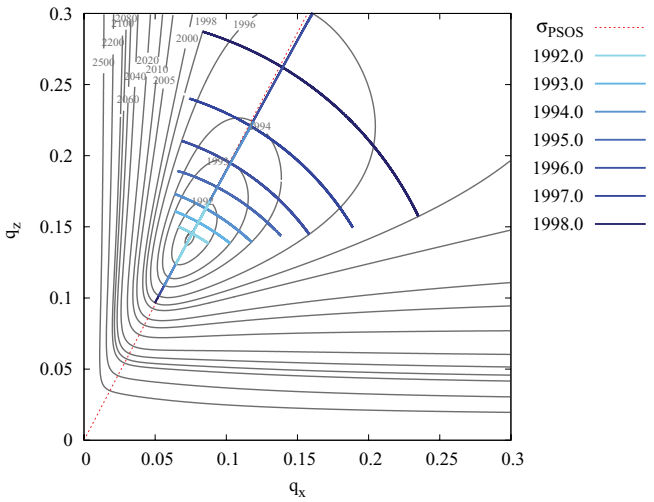

FIG. 4. (Color online) Periodic trajectories in the potential $V_{2D,h}$ at different values of energy for $\gamma_y = 2000$ and scattering length $a = 0.1$. The red dashed line denotes the surface of section for the PSOSs. There are two periodic trajectories that belong to symmetric and antisymmetric oscillations of the soliton. The symmetric oscillations are hardly visible, because they lie on top of one another and are almost parallel to the surface of section.

q_y takes nearly the value of the harmonic-oscillator ground state. As further simplification of the problem, we therefore restrict the dynamics to the plane given by the condition

$$\ddot{q}_y = \dot{p}_y \approx \frac{1}{4q_y^3} - 4\gamma_y^2 q_y \stackrel{!}{=} 0 \Rightarrow q_y = \frac{1}{2\sqrt{\gamma_y}}, \qquad (15)$$

which corresponds to a frozen Gaussian ansatz in the q_y direction. For $\gamma_y = 2000$, the plane $q_y \approx 0.011$ is marked in Fig. 1(b).

The dynamics of the wave function [Eq. (2)] with fixed parameters $A_y^r = 0$, $A_y^i = 1/8q_y^2 = \gamma_y/2$ is described in the canonical coordinates q_x and q_z by the two-dimensional potential

$$V_{2D,h}(q_x,q_z) = \frac{1}{8q_x^2} + \frac{1}{8q_z^2} + \gamma_y + \frac{\sqrt{2\gamma_y}a}{4\sqrt{\pi}q_x q_z} + \frac{1}{24\sqrt{2\pi}q_z}\left[-\frac{2\sqrt{\gamma_y}}{q_x} + \frac{1}{q_z^2} R_D\left(\frac{q_x^2}{q_z^2}, \frac{1}{4q_z^2\gamma_y}, 1\right)\right], \qquad (16)$$

which is illustrated in Fig. 4.

To describe the dynamics of this two-dimensional system, it is convenient to analyze Poincaré surfaces of section (PSOSs). For the PSOSs shown in Fig. 4, an adequate choice is to use the rotated coordinates and momenta

$$\begin{pmatrix} q_1 \\ q_2 \end{pmatrix} = \begin{pmatrix} \cos\alpha & \sin\alpha \\ -\sin\alpha & \cos\alpha \end{pmatrix} \begin{pmatrix} q_x \\ q_z \end{pmatrix}, \qquad (17a)$$

$$\begin{pmatrix} p_1 \\ p_2 \end{pmatrix} = \begin{pmatrix} \cos\alpha & \sin\alpha \\ -\sin\alpha & \cos\alpha \end{pmatrix} \begin{pmatrix} p_x \\ p_z \end{pmatrix}, \qquad (17b)$$

with $\alpha = \arctan(q_{z,\min}/q_{x,\min})$ and the crossing condition $q_2 = 0$. For constant energy, different initial conditions are integrated. The border of the allowed energy range is given by

$$p_1 = \pm\sqrt{2\left(E_{mf} - V_{2D,h}\right)}. \qquad (18)$$

In Fig. 5(a), a PSOS at an energy close to the ground state is shown. The motion is completely regular, and an elliptic fixed point of the Poincaré map is present, which belongs to the antisymmetric periodic oscillation of the condensate. The symmetric oscillation is not visible in the PSOS for the surface of section that is almost parallel to it. By increasing the energy toward $E_{mf} = \gamma_y$, the turning points of the periodic oscillations in Fig. 4 move to larger values of q_x and q_z (for the symmetric oscillation, only one turning point; for the antisymmetric, both). For $E_{mf} = \gamma_y$ they lie at infinity; i.e., the soliton dissolves. In the Poincaré map the resonant tori decay according to the Poincaré-Birkhoff theorem, building the same number of elliptic and hyperbolic fixed points in the Poincaré map. The closer to the bifurcation point the scattering length is, the lower the energy is where this takes place. This can be seen especially in Fig. 5. Further increasing of the energy leads to regions of chaotic oscillations, while the elliptic fixed point moves outward to larger values of q_1.

In the picture with a frozen Gaussian, the solitons dissolve at energy $E_{mf} = \gamma_y$ in agreement with Refs. [4,10]. If this were always true, it would imply that in an experiment with realistic parameters (e.g., a condensate with 10 000 particles at $\gamma_y = 2000$ and $a = 0.1$), the solitons must be cooled down to temperatures of about $T = 0.15\mu$K because the energy gap between the ground state and the threshold $E_{mf} = \gamma_y$ is very small (for a more detailed discussion, see Sec. IV A). However, a dynamic stabilization of the solitons at energies $E_{mf} > \gamma_y$ is possible, as will be discussed for an ansatz with a single Gaussian in Sec. II D and for coupled Gaussians in Sec. IV B.

D. Three-dimensional dynamics

In the frozen Gaussian approximation, any excitation energy of the soliton must be completely deposited in the (q_x,q_z) motion, which causes the soliton to dissolve at the low

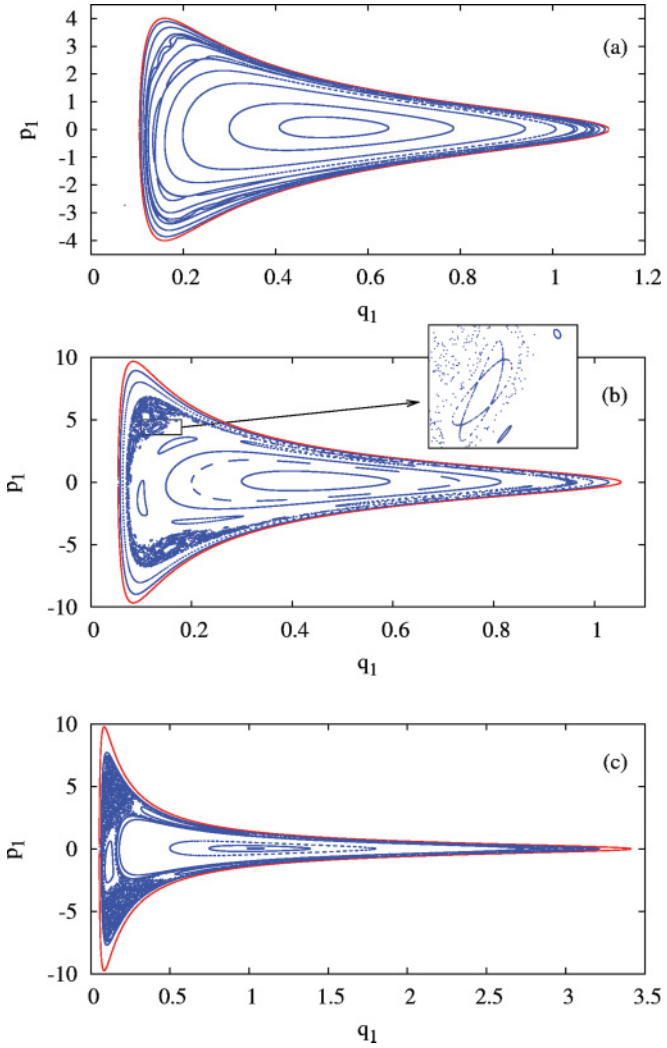

FIG. 5. (Color online) PSOSs for the dynamics of the two-dimensional potential $V_{2D,h}$ in Eq. (16) in the rotated coordinates defined in Eq. (17), with trap frequency $\gamma_y = 2000$ and (a) $a = 0.1$, $E_{\rm mf} = 1999.5$; (b) $a = 0.08$, $E_{\rm mf} = 1995$; (c) $a = 0.08$, $E_{\rm mf} = 1999$. In (a), the motion is completely regular. In (b), lowering the scattering length toward the bifurcation point causes chaotic dynamics to appear. In (c), increasing the mean-field energy close to $E_{\rm mf} = \gamma_y$ at constant scattering length enlarges the chaotic regions in the Poincaré map.

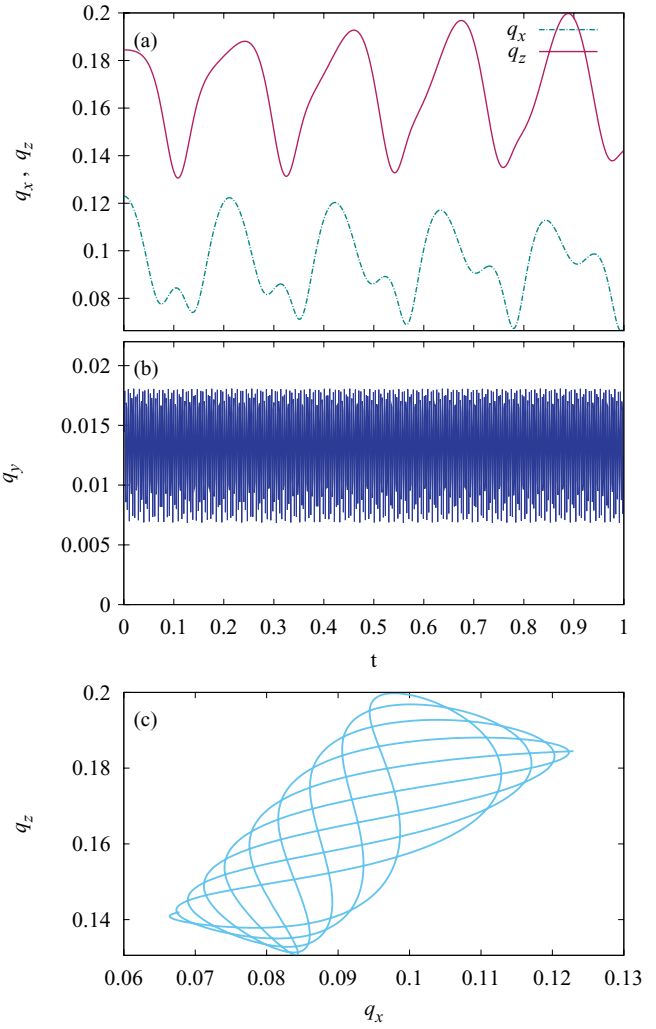

FIG. 6. (Color online) Three-dimensional trajectory of a soliton at trap frequency $\gamma_y = 2000$, scattering length $a = 0.1$, and mean-field energy $E_{\rm mf} = 3000$, far above the threshold $E_{\rm mf} = \gamma_y$, where dissolving is possible. (a,b) Time dependence of the expectation values $q_\sigma(t)$, where $\sigma = x, y, z$. (c) Lissajous-type motion of the projection in the (q_x, q_z) plane.

threshold $E_{\rm mf} = \gamma_y$. In this section we demonstrate that for the fully three-dimensional dynamics with the ansatz [Eq. (2)], a large amount of excitation energy can be stored in the q_y motion dominated by the one-dimensional harmonic trap.

An example trajectory for trap frequency $\gamma_y = 2000$, scattering length $a = 0.1$, and mean-field energy $E_{\rm mf} = 3000$, far above the threshold at γ_y, is presented in Fig. 6. In Figs. 6(a) and 6(b), the expectation values

$$q_\sigma = \sqrt{\frac{\langle \sigma^2 \rangle}{2}} = \frac{1}{8A_\sigma^i}, \quad \sigma = x, y, z \tag{19}$$

are drawn as functions of time. The slow oscillations in $q_x(t)$ and $q_z(t)$ generate the Lissajous-type motion of the quasi-two-dimensional soliton visualized in Fig. 6(c). The fast oscillation in $q_y(t)$ results primarily from the external harmonic trap. The calculations with a single Gaussian thus indicate that a rather highly excited soliton may be dynamically stabilized and does not dissolve in contrast to the calculations with a frozen Gaussian [4,10]. However, it must be clarified (see Sec. IV B) whether the dynamic stabilization is also possible with coupled Gaussians.

III. ANSATZ WITH COUPLED GAUSSIANS

Though the ansatz made in Sec. II offers a descriptive analysis of the soliton, comparison with calculations where the GPE is solved numerically on a grid show that the results for the ground state hold only qualitatively. As will be shown, the results for the dynamics of the soliton are qualitatively different as well. To gain quantitatively correct results, the ansatz for the trial function has to be modified. As shown in Refs. [6,7], the condensate wave function can be well described by a superposition of Gaussians. We therefore apply the TDVP to coupled Gaussian wave packets [11–14]. The ground state will

be determined by the ITE, with norm conservation embedded in the TDVP as a constraint.

In this section we elaborate the theory and derive the formulas for the computations with coupled Gaussians. Results for the stationary states and the dynamics of the solitons are presented in Sec. IV.

A. TDVP for GWPs

In this paper the TDVP provides the basis for solution of the time-dependent GPE. Its application to GWPs was originally introduced by Heller [15,16] for the description of atomic and molecular quantum dynamics and later applied to BECs [6,7]. For the convenience of the reader, we briefly recapitulate this method here.

The quantity

$$I = ||i\phi - H\chi(t)||^2 \stackrel{!}{=} \min \tag{20}$$

is to be minimized with respect to ϕ. Then we set $\phi \equiv \dot{\chi}$. The wave function shall be parameterized by the variational parameters $z(t)$. The variation of I in Eq. (20) carries over to the variation of z and $\dot{z}$ and results in

$$\begin{aligned}\delta I &= \langle \delta\dot{\chi}|\ \dot{\chi}\rangle + \langle \dot{\chi}|\ \delta\dot{\chi}\rangle - \langle i\delta\dot{\chi}|\ H\chi\rangle - \langle H\chi|\ i\delta\dot{\chi}\rangle \\ &= \left\langle \frac{\partial\chi}{\partial z}\delta\dot{z}\middle|\dot{\chi} + iH\chi\right\rangle + \left\langle \dot{\chi} + iH\chi\middle|\frac{\partial\chi}{\partial z}\delta\dot{z}\right\rangle,\end{aligned} \tag{21}$$

where the wave function χ is constant. Because the variational parameters are complex quantities, both brackets in Eq. (21) have to vanish separately. This yields

$$\left\langle \frac{\partial\chi}{\partial z}\middle|\frac{\partial\chi}{\partial z}\dot{z}\right\rangle = -i\left\langle \frac{\partial\chi}{\partial z}\middle|H\chi\right\rangle, \tag{22}$$

which can be written briefly as

$$K\cdot\dot{z} = -i\boldsymbol{h}, \tag{23}$$

where K is a positive-definite Hermitian matrix. The linear system [Eq. (23)] has to be solved for every time step to integrate the equations of motion $\dot{z} = f(z)$.

We now choose a linear superposition of N Gaussians as the trial function

$$\chi = \Psi = \sum_{k=1}^{N} g\left(z^k,\boldsymbol{x}\right) = \sum_{k=1}^{N} e^{i\left(\boldsymbol{x}A^k\boldsymbol{x}+\gamma^k\right)} \equiv \sum_{k=1}^{N} g^k, \tag{24}$$

where $A^k = A^{k,r} + iA^{k,i}$ are complex diagonal matrices of dimension 3×3, and $\gamma^k = \gamma^{k,r} + i\gamma^{k,i}$ denotes the relative phases and the amplitude of the Gaussians, respectively. The Gaussians are fixed at the origin. The time evolution can be considered as the motion in an effective time-dependent harmonic potential:

$$V_{\text{eff}}(\boldsymbol{x}) = v_0 + \tfrac{1}{2}\boldsymbol{x}V_2\boldsymbol{x}. \tag{25}$$

The dynamics of the GWPs are now determined by the TDVP, which variationally fits the effective time-dependent harmonic-potential coefficients v_0, V_2 to the underlying potential. Splitting the Hamiltonian $H = T + V$ and operating on the trial wave function [Eq. (24)] yields

$$\begin{aligned}i\dot{\Psi} - T\Psi = \sum_{k=1}^{N}\Big[&\underbrace{-\dot{\gamma}^k + 2i\mathrm{Tr}A^k}_{v_0^k} \\ &+\boldsymbol{x}\underbrace{\left(-\dot{A}^k - 4(A^k)^2\right)}_{\frac{1}{2}V_2^k}\boldsymbol{x}\Big]g(z^k,\boldsymbol{x}).\end{aligned} \tag{26}$$

The parameters v_0^k are scalars, and the matrices V_2^k are diagonal matrices. The equations of motion then read

$$\dot{\gamma}^k = 2i\mathrm{Tr}A^k - v_0^k, \tag{27a}$$

$$\dot{A}^k = -4(A^k)^2 - \tfrac{1}{2}V_2^k. \tag{27b}$$

The coefficients v_0^k and V_2^k have to be calculated from the TDVP:

$$\left\langle \frac{\partial g(z^k,\boldsymbol{x})}{\partial z^k}\middle|i\dot{\Psi} - H\Psi\right\rangle = 0, \tag{28}$$

$$\left\langle x_\alpha^2 g(z^l,\boldsymbol{x})\middle|\sum_{k=1}^{N}\left(v_0^k + \frac{1}{2}\boldsymbol{x}V_2^k\boldsymbol{x}\right)g(z^k,\boldsymbol{x})\right\rangle = 0. \tag{29}$$

By combining the coefficients v_0^k and V_2^k in a complex vector $\boldsymbol{v}$, the set of equations in Eq. (29) can be written as

$$K\boldsymbol{v} = \boldsymbol{r}. \tag{30}$$

The positive-definite Hermitian matrix K includes, in contrast to Eq. (23), the kinetic operator. Eq. (30) must be solved for every time step, and the resulting vector $\boldsymbol{v}$ must then be inserted in Eq. (27).

In the numerical integration of the equations of motion [Eqs. (27a) and (27b)] (e.g., with a standard algorithm like Runge-Kutta), the quadratic term can lead to numerical overflow [15]. It is therefore reasonable to split up the matrices A^k into two matrices C and B according to $A^k = B^k(C^k)^{-1}$. For the case of diagonal matrices A^k, C^k and B^k are diagonal too. Hence, the splitting can be done component by component. This leads to

$$\dot{C}^k = 4B^k; \quad \dot{B}^k = -\tfrac{1}{2}C^kV_2^k, \tag{31}$$

where $C(0) = \mathbb{1}$, and $B(0) = A(0)$ are taken as initial values.

B. Constraints in the TDVP

The most important reason for the introduction of constraints is conservation of the norm in the ITE (cf. Sec. III D). Apart from that, inequality constraints can be used to avoid matrix singularities that arise from overcrowding the basis set [17]. In principle, m constraints can be introduced, combined in the m-dimensional vector $\boldsymbol{f}$. The constraints are embedded then by a set of Lagrangian multipliers $\boldsymbol{\lambda}\in\mathbb{R}^m$:

$$L = I + \boldsymbol{\lambda}\bar{M}\dot{\bar{z}}, \tag{32}$$

where $\bar{M} = \frac{\partial f}{\partial\bar{z}}$ is a real $m\times 2n_p$ matrix. To find the minimum of I,

$$\frac{\partial L}{\partial\boldsymbol{\omega}} = 0 \quad \text{with} \quad \boldsymbol{\omega} \equiv \begin{pmatrix}\dot{z}^r\\ \dot{z}^i\\ \boldsymbol{\lambda}\end{pmatrix} = \begin{pmatrix}\dot{\bar{z}}\\ \boldsymbol{\lambda}\end{pmatrix} \in \mathbb{R}^{2n_p+m} \tag{33}$$

has to be calculated, which yields the system of equations

$$\left(\begin{array}{c|c} \bar{K} & \bar{M}^T \\ \hline \bar{M} & 0 \end{array}\right)\begin{pmatrix} \dot{\bar{z}} \\ \boldsymbol{\lambda} \end{pmatrix} = \begin{pmatrix} \bar{\boldsymbol{h}} \\ 0 \end{pmatrix}, \tag{34}$$

where

$$\bar{K} = \begin{pmatrix} K^r & -K^i \\ K^i & K^r \end{pmatrix}, \quad \bar{\boldsymbol{h}} = \begin{pmatrix} \boldsymbol{h}^i \\ -\boldsymbol{h}^r \end{pmatrix}.$$

In the special case of Gaussian wave packets, the equations of motion [split into real and imaginary parts and with the variational parameters combined to $\bar{z} = (\gamma^{1,r} \ldots \gamma^{N,r}, A^{1,r} \ldots A^{N,r}, \gamma^{1,i} \ldots \gamma^{N,i}, A^{1,i} \ldots A^{N,i})$] can be written in the form

$$\dot{\bar{z}} = \tilde{U}\bar{\boldsymbol{v}} + \tilde{\boldsymbol{d}}, \tag{35}$$

where $\tilde{U}$ consists of the terms linear in $\boldsymbol{v}$, and the constant terms are absorbed in the vector $\tilde{\boldsymbol{d}}$. The constraints combined in $\boldsymbol{f} = (f_1, \ldots, f_n)$ yield

$$\dot{\boldsymbol{f}} = \frac{\partial \boldsymbol{f}}{\partial \bar{\boldsymbol{z}}}\tilde{U}\bar{\boldsymbol{v}} + \frac{\partial \boldsymbol{f}}{\partial \bar{\boldsymbol{z}}}\tilde{\boldsymbol{d}} \equiv \bar{U}\bar{\boldsymbol{v}} + \bar{\boldsymbol{d}} = 0. \tag{36}$$

The set of linear equations [Eq. (34)] then reads

$$\left(\begin{array}{c|c} \bar{K} & \bar{U}^T \\ \hline \bar{U} & 0 \end{array}\right)\begin{pmatrix} \bar{\boldsymbol{v}} \\ \boldsymbol{\lambda} \end{pmatrix} = \begin{pmatrix} \bar{\boldsymbol{r}} \\ -\bar{\boldsymbol{d}} \end{pmatrix}, \tag{37}$$

where

$$\bar{K} = \begin{pmatrix} K^r & -K^i \\ K^i & K^r \end{pmatrix}, \quad \bar{\boldsymbol{r}} = \begin{pmatrix} \boldsymbol{r}^i \\ \boldsymbol{r}^r \end{pmatrix}. \tag{38}$$

Solving this system of linear equations and inserting the resulting vector in Eq. (27) enables one to integrate the equations of motion.

C. Energy functional

To obtain the mean-field energy of a soliton, the time-dependent variational parameters of the GWPs are used to evaluate the integrals in the energy functional. The energy functional for N coupled Gaussians reads

$$\begin{aligned} E_{\mathrm{mf}} &= \langle\Psi| - \Delta |\Psi\rangle + \langle\Psi| V_t |\Psi\rangle \\ &\quad + \tfrac{1}{2}(\langle\Psi| V_c |\Psi\rangle + \langle\Psi| V_d |\Psi\rangle). \end{aligned} \tag{39}$$

With $\sigma = x, y, z$, the integrals in Eq. (39) yield

$$\begin{aligned} \langle\Psi| - \Delta |\Psi\rangle &= \sum_{l,k}\langle g^l| - \Delta |g^k\rangle \\ &= \sum_{l,k}\left\{\left[-2i\sum_{\sigma}\left(A_\sigma^k + \frac{\left(A_\sigma^k\right)^2}{A_\sigma^{l\,*} - A_\sigma^k}\right)\right]\langle g^l|g^k\rangle\right\}, \end{aligned} \tag{40}$$

$$\langle\Psi| V_t |\Psi\rangle = -\frac{1}{2}i\sum_{l,k,\sigma}\frac{\gamma_\sigma^2}{A_\sigma^{l\,*} - A_\sigma^k}\langle g^l|g^k\rangle, \tag{41}$$

$$\begin{aligned} \langle\Psi| V_c |\Psi\rangle = 8\pi a \sum_{l,k,i,j}\Bigg[&\left(\prod_\sigma \sqrt{\frac{i\pi}{A_\sigma^k + A_\sigma^i - A_\sigma^{l\,*} - A_\sigma^{j\,*}}}\right) \\ &\times e^{i\left(\gamma^k + \gamma^i - \gamma^{l\,*} - \gamma^{j\,*}\right)}\Bigg], \end{aligned} \tag{42}$$

$$\begin{aligned} \langle\Psi| V_d |\Psi\rangle = \frac{4\pi}{3}\sum_{i,j,k,l}\Bigg[&\left(\prod_\sigma \sqrt{\frac{i\pi}{A_\sigma^k + A_\sigma^i - A_\sigma^{l\,*} - A_\sigma^{j\,*}}}\right) \\ &\times \left[\tilde{\kappa}_x\tilde{\kappa}_y R_D\left(\tilde{\kappa}_x^2, \tilde{\kappa}_y^2, 1\right) - 1\right] e^{i\left(\gamma^k + \gamma^i - \gamma^{l\,*} - \gamma^{j\,*}\right)}\Bigg], \end{aligned} \tag{43}$$

with the abbreviations

$$\tilde{\kappa}_x = \sqrt{\frac{\left(A_x^i + A_x^k - A_x^{j\,*} - A_x^{l\,*}\right)\left(A_z^i - A_z^{j\,*}\right)\left(A_z^k - A_z^{l\,*}\right)}{\left(A_x^i - A_x^{j\,*}\right)\left(A_x^k - A_x^{l\,*}\right)\left(A_z^i + A_z^k - A_z^{j\,*} - A_z^{l\,*}\right)}}$$

and

$$\tilde{\kappa}_y = \sqrt{\frac{\left(A_y^i + A_y^k - A_y^{j\,*} - A_y^{l\,*}\right)\left(A_z^i - A_z^{j\,*}\right)\left(A_z^k - A_z^{l\,*}\right)}{\left(A_y^i - A_y^{j\,*}\right)\left(A_y^k - A_y^{l\,*}\right)\left(A_z^i + A_z^k - A_z^{j\,*} - A_z^{l\,*}\right)}}.$$

The additional integrals in the TDVP—$\langle\sigma^2 V(\boldsymbol{x})\rangle$, $\langle\sigma^4 V(\boldsymbol{x})\rangle$, and $\langle\alpha^2\beta^2 V(\boldsymbol{x})\rangle$—are obtained easily from the integrals in the energy functional.

D. ITE

In principle, the ground state of the system of coupled Gaussians could be obtained by a nonlinear root search in the equations of motion. Since $4N$ complex initial values are required, it is difficult to find the fixed points in this way for a large number of Gaussians N. The ITE represents an alternative for determination of the ground state.

In the linear Schrödinger equation, the transformation $t \to \tau = it$ leads to an exponential damping of the excited states and converges to the ground state for $\tau \to \infty$. The method can be applied to the nonlinear GPE as well. In imaginary time the norm is not conserved anymore. This is crucial in the nonlinear GPE because decay of the norm indicates particle losses. To avoid norm decay, we implement norm conservation as a constraint

$$f = \sum_{k,l}\underbrace{\langle g^l|g^k\rangle}_{f_{kl}} \stackrel{!}{=} 1 \tag{44}$$

in the TDVP, as elaborated above. Supposing a general complex rotation of the time $\tau = e^{i\Omega}t$, with $\xi = \xi^r + i\xi^i = -e^{-i\Omega}$, the equations of motion can be written in the general form

$$\dot{\bar{z}} = \tilde{U}\bar{\boldsymbol{v}} + \tilde{\boldsymbol{d}}, \tag{45}$$

with

$$\tilde{U} = \begin{pmatrix} (\xi^r)_{N\times N} & (0)_{3N\times N} & (-\xi^i)_{N\times N} & (0)_{3N\times N} \\ (0)_{N\times 3N} & (\xi^r)_{3N\times 3N} & (0)_{N\times 3N} & (-\xi^i)_{3N\times 3N} \\ (\xi^i)_{N\times N} & (0)_{3N\times N} & (\xi^r)_{N\times N} & (0)_{3N\times N} \\ (0)_{N\times 3N} & (\xi^i)_{3N\times 3N} & (0)_{N\times 3N} & (\xi^r)_{3N\times 3N} \end{pmatrix},$$

$$\tilde{\boldsymbol{d}} = \xi^r \begin{pmatrix} 2\mathrm{Tr}A^{k,i} \\ 4(A^{k,r})^2 - 4(A^{k,i})^2 \\ -2\mathrm{Tr}A^{k,r} \\ 8A^{k,r}A^{k,i} \end{pmatrix} + \xi^i \begin{pmatrix} 2\mathrm{Tr}A^{k,r} \\ -8A^{k,r}A^{k,i} \\ 2\mathrm{Tr}A^{k,i} \\ 4(A^{k,r})^2 - 4(A^{k,i})^2 \end{pmatrix},$$

$$\bar{\boldsymbol{v}} = \begin{pmatrix} \boldsymbol{v}_0^r \\ \frac{1}{2}\boldsymbol{V}_2^r \\ \boldsymbol{v}_0^i \\ \frac{1}{2}\boldsymbol{V}_2^i \end{pmatrix},$$

where the abbreviated notation in $\tilde{U}$ can be understood as follows: Every entry $(\lambda)_{a\times b}$ is an $a \times b$ submatrix $\tilde{U}'$. If $\lambda = 0$, all elements of $\tilde{U}' = 0$; otherwise $\tilde{U}' = \lambda \cdot \mathbb{1}$. The vectors $\boldsymbol{v}_0^r = (v_0^{1,r}, \ldots, v_0^{N,r})^T$, $\boldsymbol{v}_0^i = (v_0^{1,i}, \ldots, v_0^{N,i})^T$, $\boldsymbol{V}_2^r = (V_2^{1,r}, \ldots, V_2^{N,r})^T$, and $\boldsymbol{V}_2^i = (V_2^{1,i}, \ldots, V_2^{N,i})^T$ contain the real and imaginary parts of the coefficients of the effective potential. The entries in $\tilde{\boldsymbol{d}}$ are vectors with the index k running from 1 to k. One special case is the real-time evolution $\xi^r = 1$, $\xi^i = 0$; the other special case is the ITE $\xi^r = 0$, $\xi^i = 1$. The gradient vector $\bar{F}^T = \partial f/\partial \bar{z}$ in Eq. (36) is given by

$$\frac{\partial f}{\partial \gamma^{k,r}} = -2\sum_{l=1}^{N} \mathrm{Im} f_{kl}, \tag{46a}$$

$$\frac{\partial f}{\partial A_\sigma^{k,r}} = -\sum_{l=1}^{N} \mathrm{Im}\frac{f_{kl}}{a_\sigma^{kl}}, \tag{46b}$$

$$\frac{\partial f}{\partial \gamma^{k,i}} = -2\sum_{l=1}^{N} \mathrm{Re} f_{kl}, \tag{46c}$$

$$\frac{\partial f}{\partial A_\sigma^{k,i}} = -\sum_{l=1}^{N} \mathrm{Re}\frac{f_{kl}}{a_\sigma^{kl}}, \tag{46d}$$

with which one obtains $\bar{U} = \bar{F}^T \cdot \tilde{U}$ and $\bar{\boldsymbol{d}} = \bar{F}^T \cdot \tilde{\boldsymbol{d}}$.

With this method the norm is conserved during the numerical integration for rather long periods of time. However, for very long periods a small drift in the norm is present because of the numerical error of the integration. The ITE of a system of ten coupled Gaussians is shown in Fig. 7.

If the relative accuracy of the integrator is chosen to be low, the mean-field energy does not decay monotonously, but for long periods it converges to the same value as an integration with a high relative accuracy; thus, a low accuracy can be chosen for the sake of time. The ITE is very robust with respect to the initial choice of the wave function. This also holds for large numbers of Gaussians coupled, where the nonlinear root search often fails. However, only the stable ground state is accessible with this method.

IV. RESULTS WITH COUPLED GAUSSIANS

By applying the variational ansatz with coupled Gaussians to the wave functions of dipolar condensates, we are now able to obtain quantitatively correct ranges of the parameters where stable quasi-two-dimensional solitons can exist. For an experimental realization of solitons with chromium atoms, realistic trap frequencies are typically a few hundred hertz for condensates with about 10 000–20 000 particles. These values

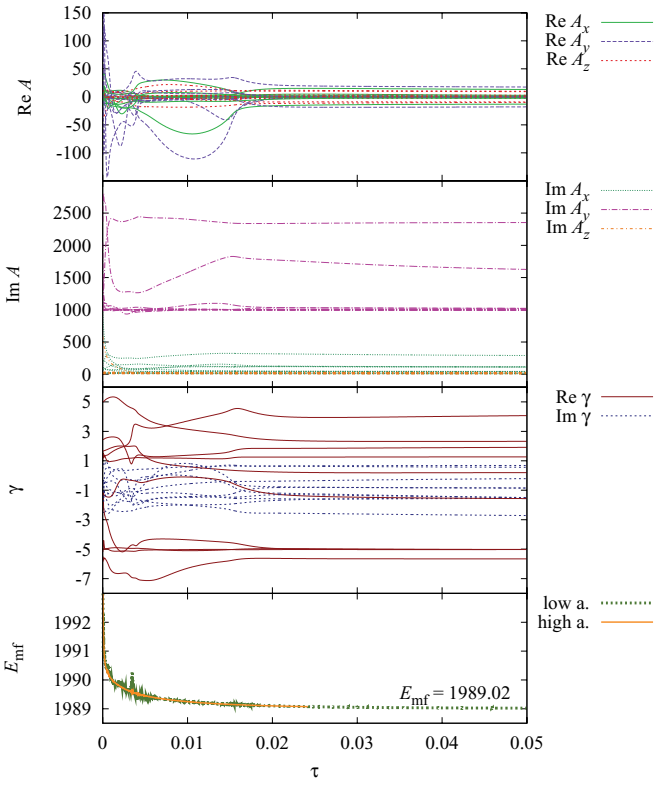

FIG. 7. (Color online) ITE of ten coupled Gaussians. The parameters used are $\gamma_y = 2000$, $a = 0.1$. Plotted are, from upper to lower panels, the real part of the width parameters, the imaginary part of the width parameters, real and imaginary parts of γ, and the mean-field energy. The mean-field energy converges to the ground state of the system as described in the text. For comparison, the mean-field energy in a fast calculation with low integration accuracy is shown as well.

roughly correspond to an interval of $2000 \lesssim \gamma_y \lesssim 20\,000$. We therefore focus our calculations on two values for the scaled trap frequency, viz., $\gamma_y = 2000$ and $\gamma_y = 20\,000$.

A. Stationary ground state

In Figs. 8 and 9 the results for the ground state of the soliton are shown at trap frequencies $\gamma_y = 2000$ and $\gamma_y = 20\,000$, respectively. In Figs. 8(a) and 9(a), the mean-field energy as a function of the scattering length is plotted for up to 6 coupled Gaussians. For comparison, the calculation using a nonlinear root search for one Gaussian, as discussed in Sec. II B, is displayed as well. The mean-field energy and the chemical potential [see Figs. 8(b) and 9(b)] converge with an increasing number of Gaussians N. The detailed convergence properties of the calculations with an increasing number of Gaussians are illustrated in Fig. 10, where calculations for up to 12 Gaussians are shown at constant scattering length $a = 0.1$. The ground-state energy converges fast with the number of Gaussians, and the corrections above a number of about five Gaussians can be neglected. The small energy differences between the variational and the grid calculations in Fig. 9(a) may be due to the finite grid size, which is limited by an acceptable computation time.

In the calculations with a single Gaussian, a stable and an unstable state are created in a tangent bifurcation at

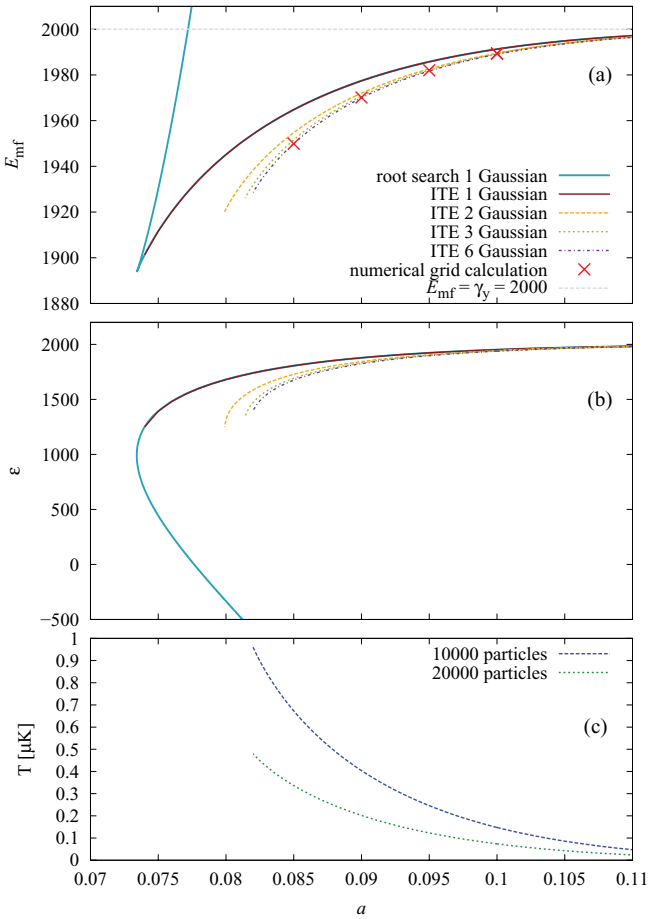

FIG. 8. (Color online) (a) Mean-field energy as a function of the scattering length of the ground state of a soliton at trap frequency $\gamma_y = 2000$, obtained by the ITE with different numbers of Gaussians. For comparison, the result for a single Gaussian obtained by a nonlinear root search and the results obtained by numerical grid calculations are plotted as well. (b) The chemical potential for the same parameters as in (a). (c) The temperature for different particle numbers belonging to the difference between upper-limit $E_{mf} = \gamma_y$ and ground-state energy.

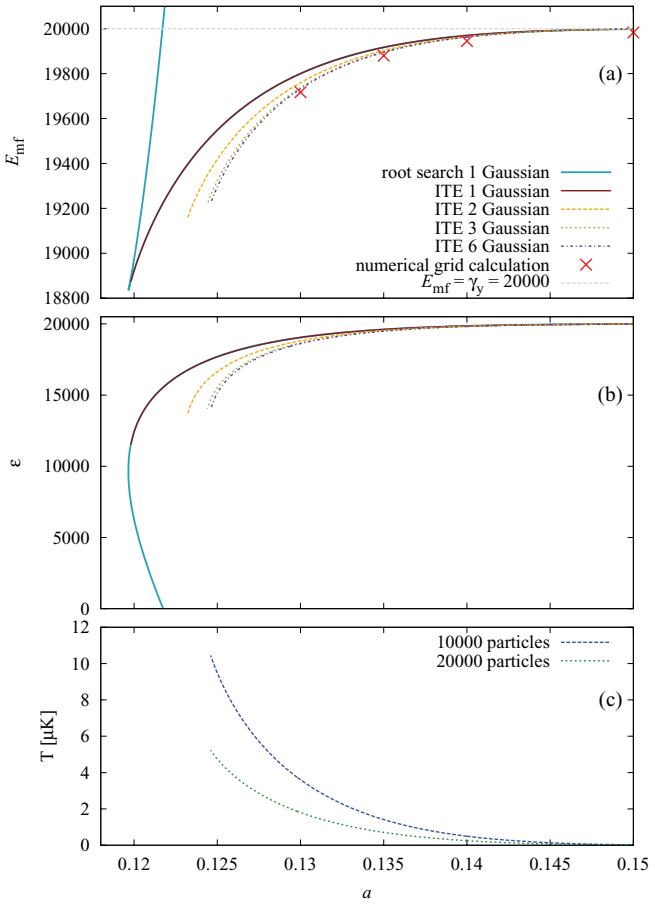

FIG. 9. (Color online) Same as Fig. 8, but for trap frequency $\gamma_y = 20\,000$. Compared to the results for $\gamma_y = 2000$, the range of the scattering length is smaller but the temperature is higher.

a scattering length $a = a_{cr}$. By using coupled Gaussians, the critical scattering length where the condensate collapses is shifted to higher values, e.g., from $a_{cr}^{N=1} = 0.0734$ to $a_{cr}^{N=6} = 0.0820$ at trap frequency $\gamma_y = 2000$, and from $a_{cr}^{N=1} = 0.1197$ to $a_{cr}^{N=6} = 0.1246$ at trap frequency $\gamma_y = 20\,000$. The ITE can provide only the stable ground state but no unstable states, which are certainly also involved in the bifurcation. For dipolar condensates in an axisymmetric trap, a complicated bifurcation scenario has been revealed [5,7], and it will be an interesting future task to study bifurcations of the soliton states in more detail.

Corrections to the calculations with a single Gaussian decrease with growing scattering lengths. This can be understood when looking at the spatial size of the soliton [cf. Fig. 2(c)]. For large expansion of the condensate, the nonlinear interaction terms in the GPE are small, and thus the mean-field energy is dominated by the ground-state energy of the harmonic trap in the y direction. Above a certain threshold value for the scattering length, the soliton is no longer bound but dissolves. The thresholds at, e.g., $a = 0.137$ for $\gamma_y = 2000$ and $a = 0.157$ for $\gamma_y = 20\,000$ obtained with a single Gaussian (see Fig. 2) are only very slightly shifted to higher values when using coupled Gaussians.

The extended variational approach allows us to compute for each trap frequency accurate lower and upper critical values of the scattering length, i.e., a range where stable solitons in dipolar BECs can exist. However, in an experiment, thermal

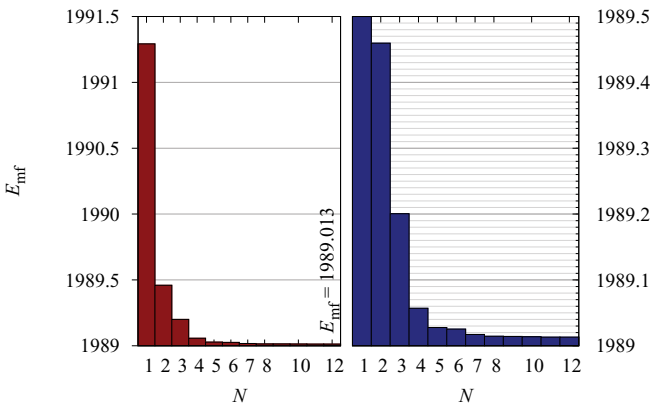

FIG. 10. (Color online) Mean-field energy for trap frequency $\gamma_y = 2000$ and fixed scattering length $a = 0.1$. The mean-field energy converges fast with an increasing number of Gaussians.

excitations of the soliton may cause the soliton to dissolve, and therefore it is also necessary to determine an energy or temperature limit for the existence of stable solitons. As a dissolving condensate without any interaction must have at least the zero-point energy $E_{\rm mf} = \gamma_y$ of the harmonic trap in the y direction, the difference between this threshold and the mean-field energy of the ground state

$$\Delta E = \gamma_y - E^g_{\rm mf} \approx \frac{3Nk_BT}{2E_d} \tag{47}$$

can be taken as a very conservative estimation of the temperature at which the soliton should survive thermal excitations. In Figs. 8(c) and 9(c), that temperature is plotted as a function of the scattering length for two condensates with $N = 10\,000$ and $N = 20\,000$ particles. With this conservative estimate, a soliton at, e.g., trap frequency $\gamma_y = 2000$ and scattering length $a = 0.1$ must be cooled down to about $T = 0.15\mu K$. However, solitons may exist at much higher temperatures when they are dynamically stabilized, as discussed in Sec. II D for the ansatz with a single Gaussian. We now extend that discussion to the ansatz with coupled Gaussians.

B. Dynamics with coupled Gaussians

The ansatz with a single Gaussian used to describe the dynamics of the solitons in Sec. II D and, especially, the further simplification with a frozen Gaussian in Sec. II C are basically mathematical model systems, and the results obtained with these models have to be seen from an academic point of view. For a realistic description it is necessary to investigate the dynamics of the solitons with the extended ansatz [Eq. (24)] of coupled Gaussians, which was shown in Sec. IV A to significantly improve the results for the ground state. Of special interest is to search for the existence of dynamically stabilized solitons at energies above the threshold $E_{\rm mf} = \gamma_y$. To this end, the equations of motion [Eqs. (27a) and (27b)] are integrated with the initial wave function chosen appropriately to yield the desired mean-field energy.

The condensate wave function [Eq. (24)] with N coupled Gaussians is parameterized by $8N$ real time–dependent variational parameters. For visualization of the wave function, we use the reduced set of parameters

$$q_\sigma = \sqrt{\tfrac{1}{2}\langle\Psi|\sigma^2|\Psi\rangle}, \quad \sigma = x,y,z, \tag{48}$$

which are related to the extension of the soliton in the three spatial dimensions and can be directly compared with the results for a single Gaussian using the coordinates in Eq. (19).

For energies close to the ground-state energy, periodic oscillations can be found. The parameters of the turning points of the periodic oscillations show a rather complicated behavior when the mean-field energy is increased. The different periodic oscillations vanish in multiple bifurcations close to the ground-state energy. Above $E_{\rm mf} = \gamma_y$, no periodic oscillations were found. However, increasing the energy above $E_{\rm mf} = \gamma_y$ yields oscillations of the soliton that do not destroy it. Applying a frozen Gaussian approximation yields stable oscillations only slightly above this limit. But allowing oscillations in all spatial directions stabilizes the condensate and gives rise to an oscillating soliton, as shown in Fig. 11 for a trajectory at trap frequency $\gamma_y = 2000$, scattering length $a = 0.1$, and mean-field energy $E_{\rm mf} = 2100$.

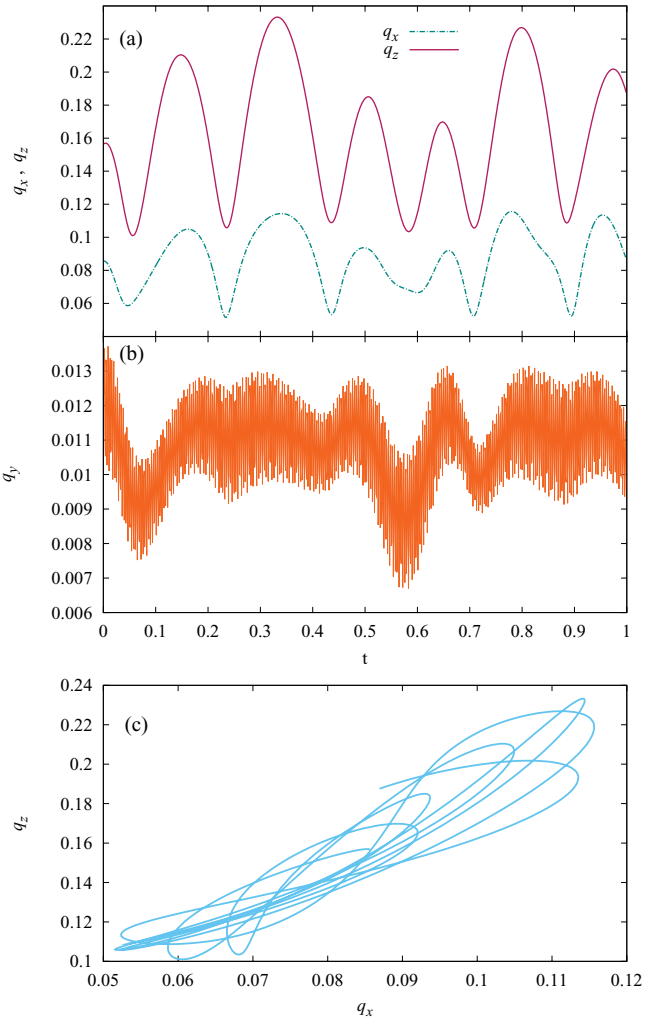

FIG. 11. (Color online) Dynamics with two coupled Gaussians for trap frequency $\gamma_y = 2000$, scattering length $a = 0.1$, and mean-field energy $E_{\rm mf} = 2100$. In (a) the parameters q_x and q_z, and in (b) the parameter q_y, in the trap direction are shown as functions of time. (c) Projection of the trajectory in the (q_x,q_z) plane. The soliton does not dissolve, although the mean-field energy is quite far above the threshold $E_{\rm mf} = \gamma_y$.

The excitation energy of the dynamically stabilized nondissolving soliton in Fig. 11 is $\Delta E = E_{\rm mf} - E^g_{\rm mf} = 111.0$, which for a condensate with 10 000 particles corresponds to a temperature of about $T = 1.5\,\mu$K. For the system with $\gamma_y = 2000$ and $a = 0.1$, stable oscillations can be found up to $E_{\rm mf} = 2400$. This is about 40 times the energy difference in Eq. (47) and yields, as an estimation of the temperature, $T = 5.5\ \mu$K for $N = 10\,000$ particles. Calculations with a higher number of coupled Gaussians and with various initial conditions show that the oscillating soliton is stable. The choice of the initial wave function is not crucial for the stability of the condensate.

V. CONCLUSION AND OUTLOOK

We investigated anisotropic quasi-two-dimensional solitons in dipolar Bose-Einstein condensates with the time-dependent variational principle by using the descriptive ansatz of both a single Gaussian wave function and coupled Gaussians to calculate the ground state of the system. The lower limit of the energy obtained with a superposition of Gaussians is in full agreement with numerical grid calculations. For a given trap frequency γ_y, we are able to give boundaries for the scattering length where stable solitons can exist. The energy gap between the mean-field energy of the ground state and the threshold energy where the soliton can dissolve is typically quite small. However, investigations of the dynamics of dipolar BECs have revealed the existence of dynamically stabilized nondissolving solitons at energies far above the threshold $E_{\mathrm{mf}} = \gamma_y$, and they open up the possibility of creating solitons at experimentally accessible temperatures [1]. This discovery may thus stimulate experiments on solitons in dipolar Bose-Einstein condensates.

ACKNOWLEDGMENTS

R.E. is grateful for support from the Landesgraduiertenförderung of the Land Baden-Württemberg.

[1] A. Griesmaier, J. Werner, S. Hensler, J. Stuhler, and T. Pfau, Phys. Rev. Lett. **94**, 160401 (2005).
[2] Q. Beaufils, R. Chicireanu, T. Zanon, B. Laburthe-Tolra, E. Maréchal, L. Vernac, J.-C. Keller, and O. Gorceix, Phys. Rev. A **77**, 061601(R) (2008).
[3] T. Lahaye, C. Menotti, L. Santos, M. Lewenstein, and T. Pfau, Rep. Prog. Phys. **72**, 126401 (2009).
[4] I. Tikhonenkov, B. A. Malomed, and A. Vardi, Phys. Rev. Lett. **100**, 090406 (2008).
[5] S. Rau, J. Main, P. Köberle, and G. Wunner, Phys. Rev. A **81**, 031605(R) (2010).
[6] S. Rau, J. Main, and G. Wunner, Phys. Rev. A **82**, 023610 (2010).
[7] S. Rau, J. Main, H. Cartarius, P. Köberle, and G. Wunner, Phys. Rev. A **82**, 023611 (2010).
[8] B. C. Carlson and J. L. Gustafson, SIAM J. Math. Anal. **25**, 288 (1994).
[9] B. C. Carlson, Numer. Algorithms **10**, 13 (1995).
[10] R. Nath, P. Pedri, and L. Santos, Phys. Rev. Lett. **102**, 050401 (2009).
[11] A. D. McLachlan, Mol. Phys. **8**, 39 (1964).
[12] E. J. Heller, J. Chem. Phys. **62**, 1544 (1975).
[13] T. Fabčič, J. Main, and G. Wunner, Phys. Rev. A **79**, 043416 (2009).
[14] T. Fabčič, J. Main, and G. Wunner, Phys. Rev. A **79**, 043417 (2009).
[15] E. J. Heller, J. Chem. Phys. **65**, 4979 (1976).
[16] E. J. Heller, J. Chem. Phys. **75**, 2923 (1981).
[17] T. Fabčič, J. Main, and G. Wunner, J. Chem. Phys. **128**, 044116 (2008).